

Deep Learning Based Model Identification System Exploits the Modular Structure of a Bio-Inspired Posture Control Model for Humans and Humanoids

Vittorio Lippi¹ ^a

¹Neurological University Clinic, University of Freiburg, Freiburg im Breisgau, Germany
vittorio.lippi@uniklinik-freiburg.de

Keywords: Posture Control, Deep Learning, System Identification, Parametric Nonlinear System

Abstract: This work presents a system identification procedure based on Convolutional Neural Networks (CNN) for human posture control using the DEC (*Disturbance Estimation and Compensation*) parametric model. The modular structure of the proposed control model inspired the design of a modular identification procedure, in the sense that the same neural network is used to identify the parameters of the modules controlling different degrees of freedom. In this way the presented examples of body sway induced by external stimuli provide several training samples at once.

1 INTRODUCTION

The application of *convolutional neural networks* (CNN) in human movement analysis has produced promising results in recent experiments (Batchuluun et al., 2018; Karatzoglou et al., 2018; Abdu-Aguye and Gomaa., 2019a; Abdu-Aguye and Gomaa., 2019b), and in general deep learning is starting to be applied to system identification (De la Rosa and Yu, 2016; Andersson et al., 2019; Miriyala and Mitra, 2020; De la Rosa et al., 2015; Ljung et al., 2020). This work aims to apply CNN to the identification of human posture control models, that are used in several studies for the analysis of human data and the control of humanoids, e.g. (van der Kooij et al., 2007; van der Kooij et al., 2005; van Asseldonk et al., 2006; Goodworth and Peterka, 2018; Mergner, 2010; Engelhart et al., 2014; Pasma et al., 2014; Jeka et al., 2010; Boonstra et al., 2014). Most of the studies on posture control use linear models like the *independent channel* (IC) model (Peterka, 2002), and make the assumption of linear and time-invariant behavior (Engelhart et al., 2016). In this work a nonlinear model will be considered. This makes the use of deep learning more interesting, as the identification of nonlinear systems is more complex and in general it is performed using computationally expensive iterative algorithms as in (Assländer et al., 2015). In a previous work, CNNs proved to be suitable to identify the parameters of a human posture control model

(Lippi. et al., 2020). Specifically, the CNN presented in (Lippi. et al., 2020) was applied to a single inverted pendulum (SIP) model, but it proved to work also in identifying the parameters of a double inverted pendulum system. In this work a triple inverted pendulum (TIP) model of posture control will be used to show how the identification process can be extended to an arbitrary number of degrees of freedom. The model used here, the *Disturbance Estimation and Compensation* (DEC) has a modular structure (Lippi and Mergner, 2017), i.e. each degree of freedom is controlled by a module and all the modules share the same structure. Exploiting this characteristic, one CNN is used to identify the parameters of the three modules controlling the three degrees of freedom. In this way each simulation provides three training samples at once.

2 METHODS

2.1 Posture Control Scenario

The scenario considered here models a human (or humanoid) balancing on a tilting support surface as a TIP. The three degrees of freedom considered in the sagittal plane are the ankles, the knees and the hips (Fig. 1A). The support surface tilt α_{FS} represents the input of the system and it is the same for all the simulations. The profile of the tilt of the support surface is the *pseudo-random ternary sequence*, PRTS, shown in Fig. 1B.

^a  <https://orcid.org/0000-0001-5520-8974>

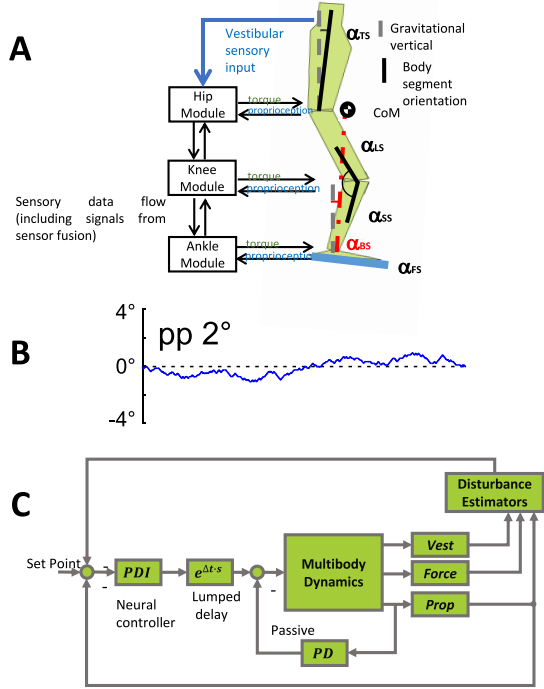


Figure 1: Balance scenario and posture control system. (A) The triple inverted pendulum model used to simulate human posture control together with the control modules. The α_{BS} represent the sway of the body COM around the ankle joint. (B) The *Pseudo-Random Ternary Signal*, PRTS, the time profile for support surface tilt. (C) Schema of a control module. The disturbances are compensated feeding them in the form of an *angle equivalent* as input to the servo controller (PID).

Such stimulus is used in human experiments because it is not predictable for the subject (Peterka, 2002). It is composed by a sequence of velocity steps suitable to excite the dynamics of the system over several frequencies. The output of the system is the sway of the body segments: shank, thigh (leg) and trunk addressed as α_{SS} , α_{LS} , and α_{TS} respectively.

2.2 Human and Humanoid Posture Control: The DEC Model

The DEC is a model of the human postural control mechanisms (Mergner, 2010; Lippi and Mergner, 2017). It has a modular structure that can be applied to multiple DoF robots (Lippi and Mergner, 2017; Zebenay et al., 2015; Ott et al., 2016; Lippi, 2018; Hettich et al., 2013; Hettich et al., 2015). Here it is implemented specifically on the TIP model, using three control modules. A block diagram of the DEC control is shown in Fig.1. A complete description of

the model is beyond the scope of this paper and can be found in (Lippi and Mergner, 2017). In the following a general description of the model is provided with particular emphasis on the components that have an impact on the definition of the machine learning problem. A control module based on the DEC concept is implemented as servo loop, here implemented as a PID controller (the neural controller in Fig. 1C). The controlled variable can consist in the COM sway of all the segments above the joint controlled by the module with respect to the gravitational vertical passing through the controlled joint (e.g. α_{BS} in Fig 1 for the ankle joint). The sensory channels shown in Fig.1 (C) as *Vestibular*, *Proprioceptive*, and *Force* are used for disturbance estimation. The disturbance estimates are fed into the servo so that the joint torque on-line compensates for the disturbances. The *lumped delay* in Fig. 1 (C) represents all the delay effects that are distributed in humans, and humanoids (Anritter et al., 2014; Hettich et al., 2014). The model used in this work considers gravity and support surface tilt as disturbances. The gravity torque to be compensated is assumed to be proportional to the sway of the COM of groups of segments above the controlled joints. Ideally the gain required to compensate gravity is mgh , where m and h are the total mass and the COM height of the controlled segments respectively, and g is the gravity acceleration. The integral component of the PID controller is not applied to the compensation as in (Ott et al., 2016). The support surface tilt estimator includes a non-linearity, introduced to represent the behavior observed in humans (Mergner et al., 2009; Mergner et al., 2003), defined as:

$$\alpha_{FS} = \int_0^t f_{\theta} \left(\frac{d}{dt} \alpha_{BS}^{vest} + \frac{d}{dt} \alpha_{BF}^{prop} \right) \quad (1)$$

where α_{BF}^{prop} is the ankle joint angle signal from proprioception. *BF* stands for *Body-to-Foot*. The function f_{θ} is a dead-band threshold defined as

$$f_{\theta}(\alpha) = \begin{cases} \alpha + \theta & \text{if } \alpha < -\theta \\ 0 & \text{if } -\theta < \alpha < \theta \\ \alpha - \theta & \text{if } \alpha > \theta \end{cases} \quad (2)$$

The estimated α_{FS} is then *up-channeled* through the control modules and used to control body position. In this work the threshold is set as $\theta = 0.0003 \text{ rad/s}$. The disturbance compensation and the total torque commanded by the servo controller for the ankle joint is:

$$\tau(s) = -e^{-s\Delta} \left(K_p + sK_d + K_i \frac{1}{s} \right) (\epsilon) + (K_p + sK_d) T_g \quad (3)$$

where K_p and K_d is the derivative coefficient for the PD controller, and Δ is the lump delay. Notice that

the derivative component is also acting on gravity T_g , representing a sort of anticipation of the disturbance. There is also a passive torque acting on the joints represented as a spring-damper model:

$$\tau_{passive} = -(K_p^{pass} + sK_d^{pass}) (\alpha_{BF}^{prop}) \quad (4)$$

The coefficients K_p^{pass} and K_d^{pass} are kept fixed for all the simulations. The standard parameters are shown in Table 1. In general the gains are proportional to the mgh for the groups of segments above the controlled joint, this will be used in the next section to normalize the parameters. The anthropometric of the TIP model is taken from previous works (Lippi et al., 2019b; Lippi and Mergner, 2020).

2.3 The Training Set

Control parameters and target set. The training set has been generated simulating the posture control scenario with different parameters, these parameters represent the target for the neural network and the sway of the segments represents the input. In order to exploit the modular structure of the DEC control the CNN has been designed to identify the parameters of a specific module. In this way each simulation provides three training samples associated with the three control modules. As explained in the previous section, the gains of the controllers are proportional to the mgh of the segments above the controlled joint, and the lumped delay is larger for the ankle module and smaller for the hip module. In order to use such parameters for the training of the same CNN their value is expressed as deviation from the default value and normalized dividing it by the default value, e.g. $\tilde{K}_p = (K_p^{sample} - K_p) / K_p$ in Table 1. Besides the PID gains the target vector includes the lumped delay and a variable C that is set to -1 when the controlled variable is the joint angle and to $+1$ when the controlled variable is the COM. This leads to a sample with the following form:

$$\tilde{T} = [\tilde{K}_p \ \tilde{K}_i \ \tilde{K}_d \ \tilde{\Delta} \ C] \quad (5)$$

where the $\tilde{\cdot}$ indicates that the values are normalized.

The training samples are generated with random parameters from normal distributions $X \sim \mathcal{N}(0, 0.5)$ that is summed to the normalized parameters. The variable C is sampled with equal probability (0.5) between the two cases. In order to avoid negative values the absolute value of the obtained parameters is used "warping" the normal distribution on positive values. A set of parameters is used as a sample only if the behavior it produces is stable: simulations with body sway larger than 6° are not considered realistic balancing scenarios and are discarded. Overall the obtained

data consist of 20730 samples, 14000 used as training set, 3000 as validation set and 3730 as test set. The three sets are normalized subtracting the average divided by the variance of the training set. The resulting distribution of the normalized \tilde{K}_p is shown in Fig. 2 together with the distribution of maximum body sway amplitudes.

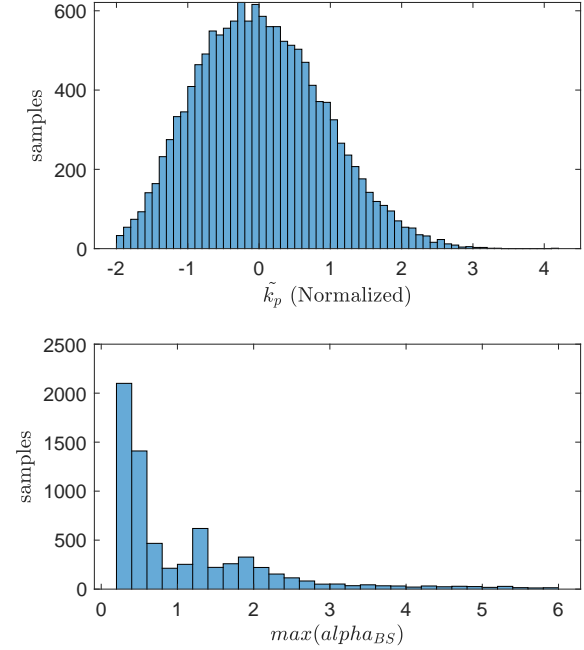


Figure 2: Output of the performed simulations. Above the distribution of the normalized \tilde{K}_p parameter produced during the stable simulations. Below the distribution of the body sway amplitudes. The last column of the histogram on the right includes the simulations that were aborted because the body sway reached the threshold of 6° .

The CNN input. The *Input* is a representation of the system output, i.e the sway of the segments. The simulation was performed with a fixed integration step of $2ms$ and sampled at $50 Hz$, producing 6051 samples with a resolution of $20 ms$. In order to adapt the signal to the CNN the input was transformed into an image. The data considered were the sway with respect to the vertical of the two segments under and above the controlled joint, e.g. for the ankle module they are α_{FS} and α_{LS} . The Spectrogram of the two signals is computed with short-time Fourier transform over windows of 250 samples overlapping for 135 computing 250 frequency points. This results in a 51×250 matrix of complex values. The first 51 columns of the matrix are here considered, corresponding to a bandwidth of approximately $10 Hz$. Due to the low-pass dynamics of the body sway, the power spectrum of the signal at higher frequency is very poor and hence not giving

Parameter	Symbol	Ankle	Knee	Hip	unit
Active proportional gain	K_p	465.98	245.25	73.575	$\frac{N \cdot m}{rad}$
Active derivative gain	K_d	116.49	18.394	18.394	$\frac{N \cdot m \cdot s}{rad}$
Active integrator gain	K_i	11.649	6.1312	1.8394	$\frac{N \cdot m}{rad \cdot s}$
Passive stiffness	$K_{p_{pass}}$	232.5000	61.2500	36.5000	$\frac{N \cdot m}{rad}$
Passive damping	$K_{d_{pass}}$	145.000	11.2500	11.2500	$\frac{N \cdot m \cdot s}{rad}$
Foot rotation velocity threshold	$\theta_{v_{fs}}$	0.03			rad/s
Lumped delay	Δ	0.10	0.07	0.1210	s

Table 1: Default parameters

important informations (i.e. almost black images independently of the parameters) . The resulting 51×51 matrix is used to define the input image as follows: the module and the phase of the matrices associated to the two segments sway are computed. The first channel of the image is the module of the matrix describing the sway of the segment above, the second is the matrix describing the segment below and the third channel is the difference between the phases. The process is summarized in Fig 3. Also the input images are normalized subtracting the average and dividing by the variance of the training set through element-wise operation (i.e. pixel by pixel, channel by channel).

2.4 CNN Architecture

The neural network architecture is schematized in Fig 4. The network is implemented with MatlabTM Deep Learning ToolboxTM. The network has been trained using *stochastic gradient descent with momentum* as policy. The training was set to a limit of 200 epochs. The loss function is the *Mean Squared Error* MSE as expected with a regression task, although the target vector includes a categorical feature, the controlled variable, that implies a classification problem. The categorical variable produced by the CNN is interpreted considering the sign (positive = COM sway, negative = joint angle). The performance in regression and classification is discussed separately in the Results section.

3 Results

3.1 Training and Test

The results of the training set are reported in Table 2. Notice that there is a total RMSE on the training set, including the error on the categorical variable, and a fit RMSE computed on the continuous variables. The average absolute error and absolute variance is shown in Fig. 5. The error is larger on K_i . The identification error in this context can be defined as the norm of the difference between body sway obtained with the target parameters (α_{BS}) and the one associated with the identified parameters ($\tilde{\alpha}_{BS}$) divided by the number of samples $N = 6051$,

$$E_{id} = \frac{\|\alpha_{BS} - \tilde{\alpha}_{BS}\|}{N} \quad (6)$$

, where the bold text represents the fact that α_{BS} is a vector of samples. The MSE on the single sample is computed considering the target error on the three control modules used in the simulation. The prediction error ϵ_p on the 15 normalized parameters is computed for each sample, leading to an MSE of

$$MSE = \sqrt{\epsilon_p^T \epsilon_p} / 15 \quad (7)$$

. The identification error plotted versus the MSE is shown in Fig. 6. On average the identification error on the training set is 0.0024°

3.2 Identification of Human Posture Control Parameters

The neural network is used to identify the control parameters from a human experiment performed with

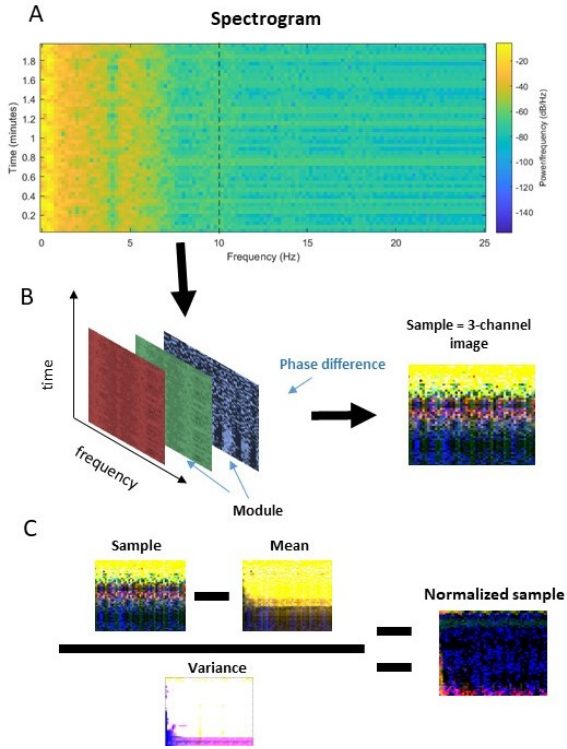


Figure 3: Design of the input features for the CNN. In A the spectrogram of a signal is given, the dashed line shows where it is cut. In B it is shown how the spectrograms associated with the sway of two body segments are combined to form a three channel 51×51 pixel image. The image C shows the normalization of the samples using the mean and the variance of the training set, computed element-wise (pixel by pixel).

Dataset	total RMSE	fit RMSE	Accuracy
Training	1.3664	1.3296	85.79%
Validation	1.5186	1.4810	83.90%
Test	1.4846	1.4486	84.72%

Table 2: Training Results

the same scenario simulated in the training set. The human experiment had the user stand with straight legs and hence the simulation was applied just to the ankle and the hip module. The identified parameters are reported in table 3 and the simulated sways of the segments are shown in Fig. 7, the result shows a good similarity between the simulation and the original data. For both the control modules, i.e. hip and ankle, the network proposed the sway in space of the segments as controlled variable, in according to previous studies on support surface tilt (Hettich et al., 2014).

Module	K_p	K_i	K_d	Δ	Var
Ankle	421.8574	74.6664	12.0254	0.0685	Sway Angle
Hip	74.5148	8.2559	1.8854	0.0219	Sway Angle

Table 3: Parameters identified for an example from a human experiment.

3.3 Identification with a *Monolithic* model

In order to evaluate the impact of the modular approach the experiment is repeated with a network that considers the three DOF together. The target vector incorporates the parameters for the 3 control modules, i.e. 15 values; the input is encoded as a 5 channel picture with with spectrograms as described in §2.3. Support surface tilt α_{FS} is not taken in account as it is the same for all the samples. The channels represent the modulus of the spectrogram for α_{LS} , α_{MS} , and α_{TS} , and the phase difference between α_{LS} and α_{MS} as well as between α_{MS} and α_{TS} . The dataset, rearranged in this way accounted for 2264 samples, i.e. one third of the original set. The dataset was split into a training set and a validation set of 1000 samples and a test set of 264 samples. The network had the same structure of the one used in the modular case, but the input and the output layers were modified according to the dimensionality of the new dataset. Such network has the disadvantage of having less training samples and more parameters, but potentially the advantage of integrating more information about the global structure of the system (e.g. distinguishing explicitly between different DOFs). The results are shown in Table 4. The performance is overall worse than in the modular

Dataset	total RMSE	fit RMSE	Accuracy
Training	4.0731	3.2723	60.20%
Validation	4.1597	3.3297	53.50%
Test	4.0531	3.2586	51.51%

Table 4: Training Results with a monolithic model

case, especially for the classification accuracy, suggesting that a modular approach is advantageous with this problem.

4 CONCLUSIONS AND FUTURE WORK

In this work a method for posture control parameter identification based on CNN is presented. The system provides an efficient way to fit a model of the non-linear bio-inspired control system DEC on experimental data. This represents an advantage with respect to previous solutions relying on iterative methods. the

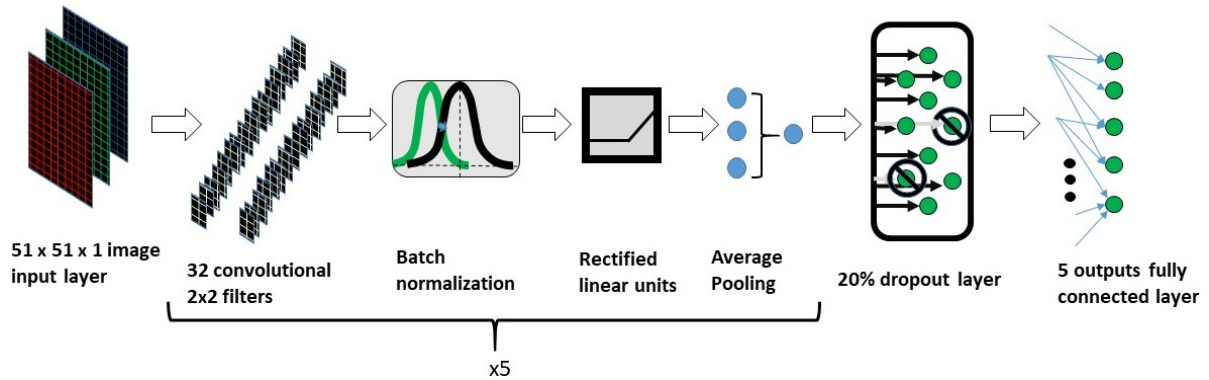


Figure 4: Neural Network architecture. The group of layers addressed with $x 5$ is repeated 5 times.

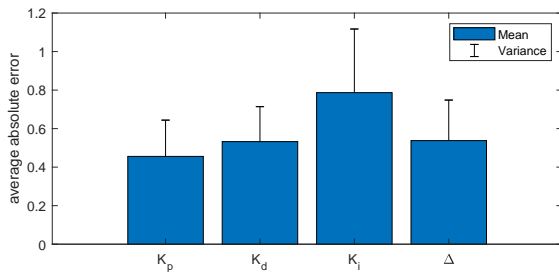


Figure 5: Average and variance of the error on the parameters.

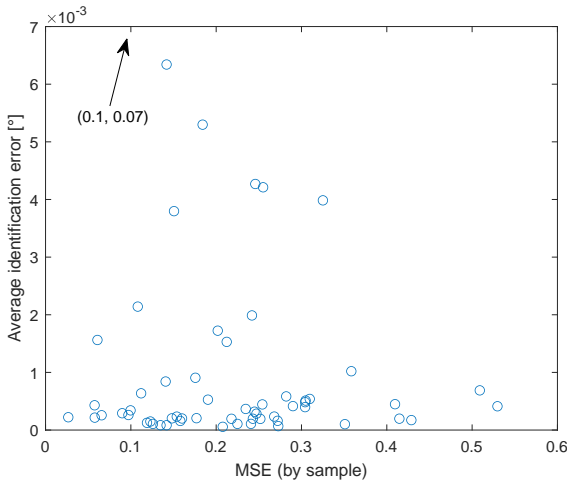


Figure 6: Identification Error for a set of 60 training samples. The identification error is plotted versus the MSE error on the parameters (target output). The arrow addresses a point that is out of the scale of the axes (i.e. MSE = 0.1, error=0.07). The correlation between the two measures of errors is -0.1265 , which means in general larger MSE on the parameters are not associated to the larger identification errors. This may suggest a certain degree of redundancy in the model, allowing the system to reproduce a similar output with different sets of parameters.

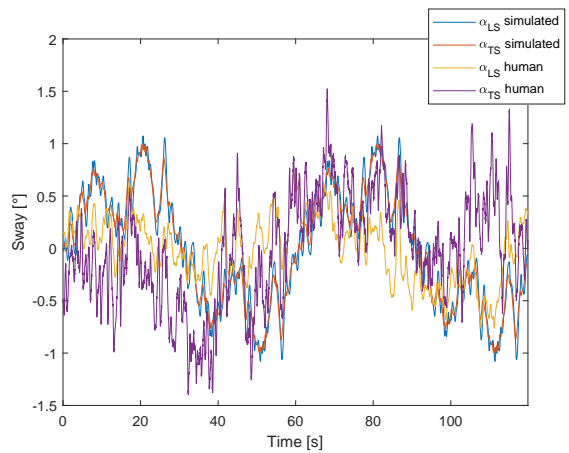


Figure 7: Human data compared with simulated responses.

training set is produced with parameters from normal distributions (although only the parameters producing a stable simulation are selected). Future work will focus on the distribution of human data. An *a posteriori* test can be performed comparing the distribution of the parameters identified on the test set with the expected distribution on real data. This can help the process of choosing between different possible network hyperparameters sets as shown in (Sforza et al., 2011; Sforza and Lippi, 2013).

Some parameters were better identified than others as shown in Fig. 5. This may be due to the kind of experimental set up or due to the choice of the input features. For example the effect of K_i is mainly visible just in the low pass components of the spectrogram. Furthermore, simulations and robot experiments are able to reproduce human behavior in the considered set up (PRTS support surface tilt) without the integral component of the neural controller (Mergner, 2010; Hettich et al., 2015; Hettich et al., 2014). The integral component of the controller is more important in analyzing transient behavior, e.g. reaching a desired

position, where it can be used to guarantee zero tracking error (Ott et al., 2016). A tracking task may be better to identify K_i more precisely.

The proposed CNN for posture control modeling can find application in bio-inspired humanoid control, e.g. (Choi and Kim, 2007; Abedi and Shoushtari, 2012; Zebenay et al., 2015; Mergner and Lippi, 2018). The CNN can also be helpful in setting up wearable robots using the control parameters identified on the user (Chugo et al., 2019; Mergner and Lippi, 2019). The parameters can be a tool to benchmark humanoids and wearable devices (Torricelli et al., 2020), in particular, in the framework of the COMTEST project (Lippi et al., 2019a; Lippi et al., 2020) that aims to make a posture control testbed available for the humanoid robotics community, and to define performance metrics.

ACKNOWLEDGEMENTS



This work is supported by the project COMTEST, a sub-project of EUROBENCH (European Robotic Framework for Bipedal Locomotion Benchmarking, www.eurobench2020.eu) funded by H2020 Topic ICT 27-2017 under grant agreement number 779963.

REFERENCES

- Abdu-Aguye, M. G. and Gomaa, W. (2019a). On the feasibility of on-body roaming models in human activity recognition. In *Proceedings of the 16th International Conference on Informatics in Control, Automation and Robotics - Volume 1: ICINCO*, pages 507–516. INSTICC, SciTePress.
- Abdu-Aguye, M. G. and Gomaa, W. (2019b). Versatl: Versatile transfer learning for imu-based activity recognition using convolutional neural networks. In *Proceedings of the 16th International Conference on Informatics in Control, Automation and Robotics - Volume 1: ICINCO*, pages 507–516. INSTICC, SciTePress.
- Abedi, P. and Shoushtari, A. L. (2012). Modelling and simulation of human-like movements for humanoid robots. In *Proceedings of the 9th International Conference on Informatics in Control, Automation and Robotics - Volume 1: ICINCO*, pages 342–346. INSTICC, SciTePress.
- Andersson, C., Ribeiro, A. H., Tiels, K., Wahlström, N., and Schön, T. B. (2019). Deep convolutional networks in system identification. In *2019 IEEE 58th Conference on Decision and Control (CDC)*, pages 3670–3676. IEEE.
- Anritter, F., Scholz, F., Hettich, G., and Mergner, T. (2014). Stability analysis of human stance control from the system theoretic point of view. In *Control Conference (ECC), 2014 European*, pages 1849–1855. IEEE.
- Assländer, L., Hettich, G., and Mergner, T. (2015). Visual contribution to human standing balance during support surface tilts. *Human movement science*, 41:147–164.
- Batchuluun, G., Naqvi, R. A., Kim, W., and Park, K. R. (2018). Body-movement-based human identification using convolutional neural network. *Expert Systems with Applications*, 101:56–77.
- Boonstra, T. A., van Vugt, J. P., van der Kooij, H., and Bloem, B. R. (2014). Balance asymmetry in parkinson’s disease and its contribution to freezing of gait. *PLoS One*, 9(7):e102493.
- Choi, Y. and Kim, D. (2007). On the balancing control of humanoid robot. In *Proceedings of the Fourth International Conference on Informatics in Control, Automation and Robotics - Volume 2: ICINCO*, pages 248–252. INSTICC, SciTePress.
- Chugo, D., Koyama, M., Yokota, M., Kawazoe, S., Muramatsu, S., Yokota, S., Hashimoto, H., Katayama, T., Mizuta, Y., and Koujina, A. (2019). Sitting assistance that considers user posture tolerance. In *Proceedings of the 16th International Conference on Informatics in Control, Automation and Robotics - Volume 2: ICINCO*, pages 489–496. INSTICC, SciTePress.
- De la Rosa, E. and Yu, W. (2016). Randomized algorithms for nonlinear system identification with deep learning modification. *Information Sciences*, 364:197–212.
- De la Rosa, E., Yu, W., and Li, X. (2015). Nonlinear system identification using deep learning and randomized algorithms. In *2015 IEEE International Conference on Information and Automation*, pages 274–279. IEEE.
- Engelhart, D., Boonstra, T. A., Aarts, R. G., Schouten, A. C., and van der Kooij, H. (2016). Comparison of closed-loop system identification techniques to quantify multi-joint human balance control. *Annual reviews in control*, 41:58–70.
- Engelhart, D., Pasma, J. H., Schouten, A. C., Meskers, C. G., Maier, A. B., Mergner, T., and van der Kooij, H. (2014). Impaired standing balance in elderly: a new engineering method helps to unravel causes and effects. *Journal of the American Medical Directors Association*, 15(3):227–e1.
- Goodworth, A. D. and Peterka, R. J. (2018). Identifying mechanisms of stance control: a single stimulus multiple output model-fit approach. *Journal of neuroscience methods*, 296:44–56.
- Hettich, G., Assländer, L., Gollhofer, A., and Mergner, T. (2014). Human hip—ankle coordination emerging from multisensory feedback control. *Human Movement Science*, 37:123–146.
- Hettich, G., Lippi, V., and Mergner, T. (2013). Human-like sensor fusion mechanisms in a postural control robot. In Londral, A. E., Encarnacao, P., and Pons, J. L., editors, *Proceedings of the International Congress on Neurotechnology, Electronics and Informatics. Vilamoura, Portugal*, pages 152–160.

- Hettich, G., Lippi, V., and Mergner, T. (2015). Human-like sensor fusion implemented in the posture control of a bipedal robot. In *Neurotechnology, Electronics, and Informatics*, pages 29–45. Springer.
- Jeka, J. J., Allison, L. K., and Kiemel, T. (2010). The dynamics of visual reweighting in healthy and fall-prone older adults. *Journal of motor behavior*, 42(4):197–208.
- Karatzoglou, A., Schnell, N., and Beigl, M. (2018). A convolutional neural network approach for modeling semantic trajectories and predicting future locations. In *International Conference on Artificial Neural Networks*, pages 61–72. Springer.
- Lippi, V. (2018). Prediction in the context of a human-inspired posture control model. *Robotics and Autonomous Systems*.
- Lippi, V. and Mergner, T. (2017). Human-derived disturbance estimation and compensation (dec) method lends itself to a modular sensorimotor control in a humanoid robot. *Frontiers in neurobotics*, 11:49.
- Lippi, V. and Mergner, T. (2020). A challenge: Support of standing balance in assistive robotic devices. *Applied Sciences*, 10(15):5240.
- Lippi, V., Mergner, T., and Maurer, C. (2020). Deep learning for posture control nonlinear model system and noise identification. In *Proceedings of the 17th International Conference on Informatics in Control, Automation and Robotics - Volume 1: ICINCO*, pages 607–614. INSTICC, SciTePress.
- Lippi, V., Mergner, T., Maurer, C., and Seel, T. (2020). Performance indicators of humanoid posture control and balance inspired by human experiments. In *The International Symposium on Wearable Robotics (WeRob2020) and WearAcon Europe*.
- Lippi, V., Mergner, T., Seel, T., and Maurer, C. (2019a). COMTEST project: A complete modular test stand for human and humanoid posture control and balance. In *2019 IEEE-RAS 19th International Conference on Humanoid Robots (Humanoids) Toronto, Canada. October 15-17*.
- Lippi, V., Molinari, F., and Seel, T. (2019b). Distributed bio-inspired humanoid posture control. In *2019 41st Annual International Conference of the IEEE Engineering in Medicine and Biology Society (EMBC)*, pages 5360–5365. IEEE.
- Ljung, L., Andersson, C., Tiels, K., and Schön, T. B. (2020). Deep learning and system identification. In *21st IFAC World Congress*, page 8.
- Mergner, T. (2010). A neurological view on reactive human stance control. *Annual Reviews in Control*, 34(2):77–198.
- Mergner, T. and Lippi, V. (2018). Posture Control–Human-Inspired Approaches for Humanoid Robot Benchmarking: Conceptualizing Tests, Protocols and Analyses. *Frontiers in Neurobotics*, 12:21.
- Mergner, T. and Lippi, V. (2019). Integrating posture control in assistive robotic devices to support standing balance. In Carrozza M., Micera S., P. J., editor, *Wearable Robotics: Challenges and Trends. WeRob 2018*, volume 22 of *Biosystems & Biorobotics*. Springer, Cham.
- Mergner, T., Maurer, C., and Peterka, R. J. (2003). A multi-sensory posture control model of human upright stance. *Progress in Brain Research*, 142:189–201.
- Mergner, T., Schweigart, G., and Fennell, L. (2009). Vestibular humanoid postural control. *Journal of Physiology - Paris*, 103:178–194.
- Miriyala, S. S. and Mitra, K. (2020). Deep learning based system identification of industrial integrated grinding circuits. *Powder Technology*, 360:921–936.
- Ott, C., Henze, B., Hettich, G., Seyde, T. N., Roa, M. A., Lippi, V., and Mergner, T. (2016). Good posture, good balance: Comparison of bioinspired and model-based approaches for posture control of humanoid robots. *IEEE Robotics & Automation Magazine*, 23(1):22–33.
- Pasma, J., Engelhart, D., Schouten, A., Van der Kooij, H., Maier, A., and Meskers, C. (2014). Impaired standing balance: the clinical need for closing the loop. *Neuroscience*, 267:157–165.
- Peterka, R. (2002). Sensorimotor integration in human postural control. *Journal of neurophysiology*, 88(3):1097–1118.
- Sforza, F. and Lippi, V. (2013). Support vector machine classification on a biased training set: Multi-jet background rejection at hadron colliders. *Nuclear Instruments and Methods in Physics Research Section A: Accelerators, Spectrometers, Detectors and Associated Equipment*, 722:11–19.
- Sforza, F., Lippi, V., and Chiarelli, G. (2011). Rejection of multi-jet background in $pp \rightarrow ev + jj$ channel through a svm classifier. In *Journal of Physics: Conference Series*, volume 331, pages 32–45. IOP Publishing.
- Torricelli, D., Mizanoor, R. S., Lippi, V., Weckx, M., Mathijssen, G., Vanderborght, B., Mergner, T., Lefebvre, D., and Pons, J. L. (2020). Benchmarking human likeness of bipedal robot locomotion: State of the art and future trends. In *Metrics of Sensory Motor Coordination and Integration in Robots and Animals*, pages 147–166. Springer.
- van Asseldonk, E. H., Buurke, J. H., Bloem, B. R., Renzenbrink, G. J., Nene, A. V., van der Helm, F. C., and van der Kooij, H. (2006). Disentangling the contribution of the paretic and non-paretic ankle to balance control in stroke patients. *Experimental neurology*, 201(2):441–451.
- van der Kooij, H., van Asseldonk, E., and van der Helm, F. C. (2005). Comparison of different methods to identify and quantify balance control. *Journal of neuroscience methods*, 145(1-2):175–203.
- van der Kooij, H., van Asseldonk, E. H. F., Geelen, J., van Vugt, J. P. P., and Bloem, B. R. (2007). Detecting asymmetries in balance control with system identification: first experimental results from parkinson patients. *Journal of Neural Transmission*, 114(10):1333.
- Zebenay, M., Lippi, V., and Mergner, T. (2015). Human-like humanoid robot posture control. In *2015 12th International Conference on Informatics in Control, Automation and Robotics (ICINCO)*, volume 2, pages 304–309. INSTICC, SciTePress.